




Construction and evaluation of a prognostic model of autophagy-related genes in hepatocellular carcinoma

Yutao He¹, Bin Du¹, Weiran Liao¹, Wei Wang, Jifeng Su, Chen Guo, Kai Zhang, Zhitian Shi^{*} 

Department of Hepatobiliary and Pancreatic Surgery, The Second Affiliated Hospital of Kunming Medical University, No.374 Yunnan-Burma Road, Kunming, Yunnan, 650101, China

ARTICLE INFO

Keywords:

Hepatocellular cancer (HCC)
Autophagy
Prognosis
Risk model

ABSTRACT

Background: Hepatocellular carcinoma (HCC) is a globally prevalent disease. Our article evaluates risk models based on autophagy- and HCC-related genes and their prognostic value by bioinformatics analytical methods to provide a scientific basis for clinical treatment.

Methods: Prognostic genes were identified by univariate and multivariate Cox analyses, and risk scores were calculated. The value of risk models was analysed by receiver operating characteristic curve (ROC), immune microenvironment and drug sensitivity. Prognostic gene-related regulatory mechanisms based on network database.

Results: We screened four prognosis-related genes (SQSTM1, GABARAPL1, CDKN2A, HSPB8) for model construction. The AUC for 1-, 2- and 3-year survival was higher than 0.6 in both the training and validation sets. The nomogram constructed based on risk scores, pathologic_T predicted the outcome better. There were differences in the tumour microenvironment between the high and low risk groups, as evidenced by differences in the distribution of immune cells and differences in the expression of immune checkpoints.

Conclusion: Our results illustrate that models, nomograms and risk scores were valuable for tumour progression. **Clinical trial number:** Not applicable.

1. Introduction

Liver cancer is a frequent cancer in the digestive system and hepatocellular carcinoma (HCC) is its main histological type, accounting for about 70–80% of cases [1]. According to the data from the International Agency For Research on Cancer (IARC) 2020 [2], HCC is a highly prevalent malignancy with a global incidence of more than 90 million people. HCC even ranks among the top three of all cancers in terms of mortality. Both liver fibrosis and cirrhosis are precursors to HCC [3]. Chronic infection with hepatitis B virus (HBV) or hepatitis C virus (HCV), excessive and sustained intake of foods containing nitrosamines, alcohol, etc., and nonalcoholic fatty liver disease (NAFLD) are all potential triggers of cirrhosis [4,5].

HCC is highly invasive and heterogeneous, with metastasis and recurrence in most cases, presenting an unsatisfactory prognosis. Articles [6] have shown that the 5-year survival rate is usually less than 20% [7]. Early interventions such as radiotherapy, chemotherapy and surgical resection can improve the 5-year survival rate to more than 30%,

but the results are still unsatisfactory, and there is a high recurrence rate. To date, TNM tumour staging, histology and other modalities have been commonly used in the clinic to assess the prognosis of HCC. α -Fetoprotein (AFP) is the most widely used as a serum marker. Although it helps to improve the prognosis, patients with HCC still need more accurate biomarkers to improve the risk prediction of HCC and thus improve the prognosis. Recently, a large number of studies have validated HCC-related prognostic models. For example, the article [8] constructed a risk score model that could successfully predict the 1-year recurrence rate of HCC patients. Through machine learning, the study built predictive survival and clinically relevant models for evaluating candidate markers [9]. Therefore, the establishment of more reliable predictive models and in-depth studies could provide important information for clinical treatment.

Autophagy is a process due to the catabolism of cells under externally stimulated conditions. Autophagy participates in organelle renewal, which maintains the integrity of proteinaceous material and organelles, thus maintaining the stability of the cell in its roles of survival,

* Corresponding author.

E-mail address: sztkmmu@163.com (Z. Shi).

¹ Contributed equally.

differentiation and regulation [10]. Due to the role of autophagy, its dysfunction has been shown to be closely associated with the development of a variety of diseases especially in cancer. In recent years, the discussion of autophagy in cancer has been complex and controversial. This is due to the large number of genes associated with autophagy. Autophagy has the ability to remove harmful cells, and some of its related genes exhibit cancer suppression. Then, the absence of some genes promotes the development of cancer. For example, some articles demonstrated that Beclin 1 is lowly expressed in prostate, breast, and ovarian cancers, and its deletion promotes tumour proliferation [11,12]. Down-regulation of Bif-1 promotes melanoma growth [13]. Other studies have shown that the metabolic sensitivity of autophagy plays an oncogenic role. In glioblastoma (GBM), autophagy promotes its invasive and drug resistance [14,15]. Thus, autophagy has a different role in different stages and tissues of cancer. It is imperative to study its underlying biological mechanisms.

In this study, we first analysed datasets from The Cancer Genome Atlas (TCGA) and International Cancer Genome Consortium (ICGC) to screen and identify differentially expressed genes associated with autophagy, followed by the development of a risk model, which was assessed to accurately predict patient prognosis. The regulatory network, immune infiltration and drug sensitivity of key genes were subsequently analysed. Finally, we formalised that these key genes have great potential and research value in HCC.

2. Materials and Methods

2.1. Data source

TCGA training set: HCC gene expression matrices and clinical traits were downloaded from the TCGA database from UCSC Xena (<https://xena.ucsc.edu/public/>) for a total of 424 samples, of which 01A (HCC, 369 samples) and 11A (Control, 50 samples) samples were used for the analyses; among the HCC samples, there were 363 samples that contained survival information.

Validation set: ICGC-LIRI-JP was downloaded from the ICGC (International Cancer Genome Consortium) database (<https://dcc.icgc.org/projects/LIRI-JP#!>) for gene expression data and survival information for 232 HCC samples, which were used to validate the accuracy of the prognostic model.

Immune checkpoints: In the literature [16] 17 receptors, 16 ligands, 3 cell adhesion, 3 co-stimulators, 14 antigens, 7 co-suppressors and 5 other relevant immune checkpoints were obtained.

Autophagy-associated genes: A total of 222 autophagy-associated genes were obtained from the Human Autophagy Genebank (HADb, <http://www.autophagy.lu/index.html>) (Supplementary Table 1).

2.2. Differential expression analysis

Differential expression analysis was performed using the DESeq2 (version 1.38.3) [17] to screen for significantly differentially expressed genes (DEGs). Significant differentially expressed genes were screened by $|\log_2FC| \geq 1$ and $p\text{-adj} < 0.05$. Visualisation was performed by using ggplot2 (version 3.3.6) [18] and ComplexHeatmap (version 2.14.0) [19]. Venn was shown by using UpSetR (version 1.4.0) [20] to obtain intersecting genes.

2.3. GO and KEGG

The clusterProfiler (version 4.4.4) [21] was used for ID conversion, followed by GO and KEGG enrichment analyses ($p\text{-value} < 0.05$) and finally visualised by using the ggplot2 package (version 3.3.6).

2.4. Protein-protein interaction (PPI)

The STRING (<https://cn.string-db.org/>) database was used to

construct protein-interaction networks. Cytoscape (version 3.9.1) was used to construct network graphs, and concepts from reference articles [22] were used to construct networks.

2.5. Risk modelling and assessment

Autophagy-related genes with prognostic impact on HCC were screened by Cox regression analysis with the survival (version 3.4.0) [23] and survminer package (version 0.4.9) [24], followed by further screening of genes that could be used to construct risk models by proportional risk assumption test and multifactorial Cox. The risk score calculation formula was shown below.

$$\text{riskScore} = \beta_1X_1 + \beta_2X_2 + \dots + \beta_nX_n$$

β denotes Cox regression coefficient and X denotes gene expression. Subsequently, the genes were divided into high-risk and low-risk groups based on the median value of the risk score. Finally, the survival rate of patients between the two groups was compared by Kaplan-Meier curve ($p < 0.05$). The predictive ability of the genes was assessed by plotting the results at 1/2/3 years through the receiver operating characteristic curve (ROC) curve and comparing the area under the curve (AUC) by survivalROC (version 1.0.3.1) [25]. AUC closer to 1 indicates better recognition ability. AUC = 0.5 is a randomised classification, at which point the identification ability is not available.

2.6. Nomogram construction

The reliability of the model was further assessed on the basis of clinical traits, and significant clinical traits were obtained by Cox analysis for the construction of nomogram and DCA correction curves. Nomograms were drawn using the survival and rms (version 6.3.0) [26] packages to predict 1-, 2-, and 3-year patient survival. Correction curves were plotted using ggDCA (version 1.2) [27], with closer to 45° indicating better prediction.

2.7. Gene set enrichment analysis

The KEGG gene set was downloaded as the background set using the msigdb package (version 7.5.1) [28] in R. And the sequenced genes were enriched in the background gene set using the GSEA function ($\text{adj. } p < 0.05$), and the enrichment results were represented by the enrichplot package (version 1.16.2) [29].

2.8. Tumour microenvironment analysis

The ESTIMATE algorithm (version 1.0.13) [29] was used to calculate the StromalScore, ImmuneScore and these two scores were added together to obtain the ESTIMATEScore. Differences between subgroups were analysed according to $p < 0.05$. Samples in the training set were analysed using GSVA (version 1.44.5) [30] to obtain enrichment scores for 28 immune cells using the immune-related genes provided in the literature [31] as the background gene set. The Wilcoxon test was used to analyse between-group differences in immune cell enrichment scores. Correlations between prognostic genes, risk scores and differential immune cell enrichment scores were analysed using the Spearman analysis. Finally, the differences in the expression of each immune checkpoint between the groups were analysed using the Wilcoxon test.

2.9. Stemness index and drug sensitivity analysis

The stemness index between tumour samples was calculated using the synapser package (version 1.1.0) [32]. Models were constructed using the v2 version of data from the GDSC (Genomics of Drug Sensitivity in Cancer) database as a training set (805 cell lines, 17,419 genes, 198 drugs) to predict the IC₅₀ values (the half inhibitory concentration of the antagonist being measured) by oncoPredict (version 0.2) [33].

Table 1
Primer sequence.

Gene	Forward Primer (5'-3')	Reverse Primer (5'-3')
CDKN2A	GATCCAGGTGGGTAGAAGGTC	CCCCTGCAAACCTTGGTCCT
GABARAPL1	ATGAAGTTCAGTACAAGGAGGA	GCTTTTGGAGCCTTCTCTACAAT
HSPB8	CTCCTGCCACTACCCAAGC	GGCCAAGAGGCTGTCAAGT
SQSTM1	GCACCCCAATGTGATCTGC	CGCTACACAAGTCGTAGTCTGG

Correlations were assessed by Spearman correlation analysis.

2.10. Transcription factor prediction and ceRNA analysis

TFs associated with 4 prognostic genes were predicted by using miRNet (<https://www.mirnet.ca/>) based on the RegNetwork database (<https://regnetworkweb.org/>) with degree ≥ 1 . Associated regulatory networks were mapped using Cytoscape (version 3.9.1) [34]. The StarBase database (<http://starbase.sysu.edu.cn/starbase2/>) was used to predict gene-associated miRNAs, lncRNAs, and construct related networks.

2.11. Clinical sample

Tissue samples from 10 HCC patients and paracancerous tissue samples were obtained from the Second Affiliated Hospital of Kunming Medical University. The samples were histologically characterized. The study was approved by the Ethics Committee of the Second Affiliated Hospital of Kunming Medical University (PJ-2024-147). All samples met the requirements of medical ethics (Declaration of Helsinki). The patients agreed and signed an informed consent form.

2.12. Western blotting

The tissue was lysed using RIPA lysis solution (Sigma, USA). The supernatant was extracted after centrifugation at 12,000 g at 4 °C. Proteins were separated using SDS-PAGE and transferred to a PVDF membrane. Incubate with primary antibody after sealing using BSA. Antibody information was shown below, anti-CDKN2A (Abcam, ab270058, 1:1000), anti-GABARAP1 (Abcam, ab109364, 1:1000), anti-HSPB8 (Abcam, ab151552, 1:1000), anti-SQSTM1 (Abcam, ab207305, 1:1000). Quantitative analysis of the grey values of the bands was performed using ImageJ.

2.13. Immunohistochemistry (IHC)

Tissues were preserved in 4 % paraformaldehyde. Serial 4 μm sections of the sample tissue were used to prepare paraffin. After baking the paraffin sections, the paraffin sections were dehydrated and antigenically repaired. Primary antibody was added and they were incubated at 37 °C. Tissue sections were then stained with diaminobenzidine (Beyotime, China) and hematoxylin (Beyotime, China) for colour development. The results were quantitatively analysed using ImageJ as described in the article. Antibody information was shown below, anti-CDKN2A (Abcam, ab270058, 1:500), anti-GABARAP1 (Abcam,

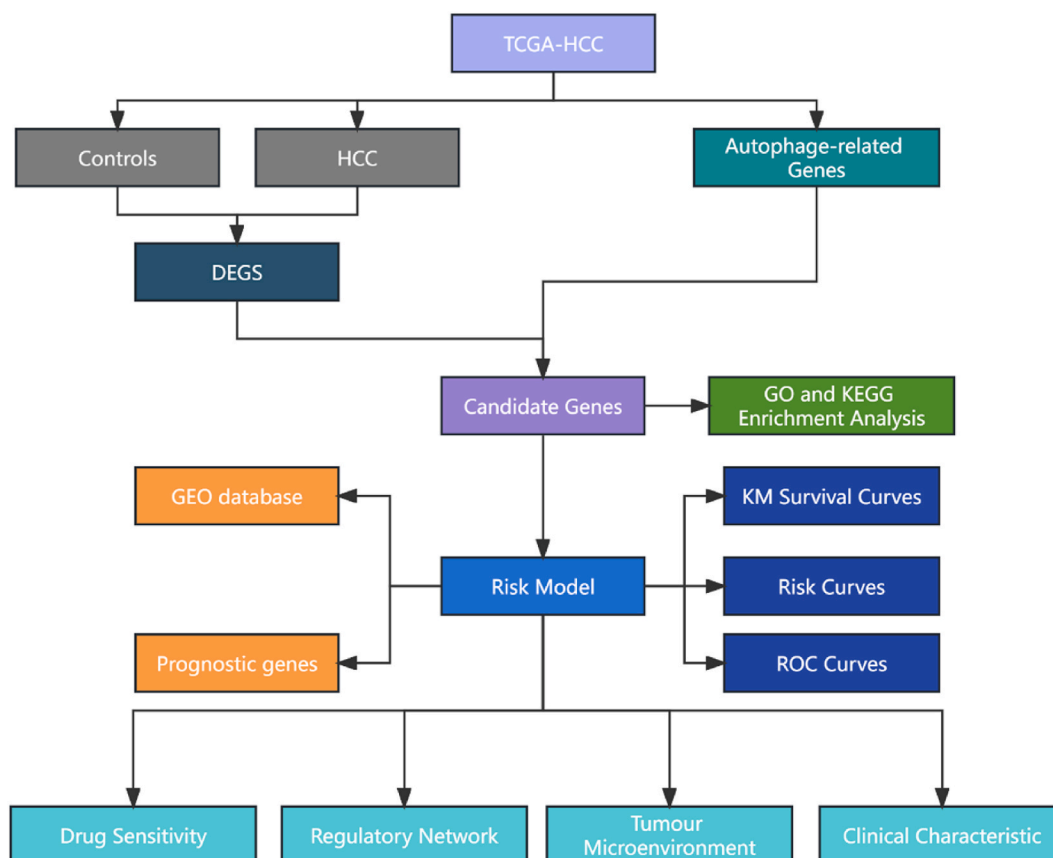


Fig. 1. Flowchart of design for this study.

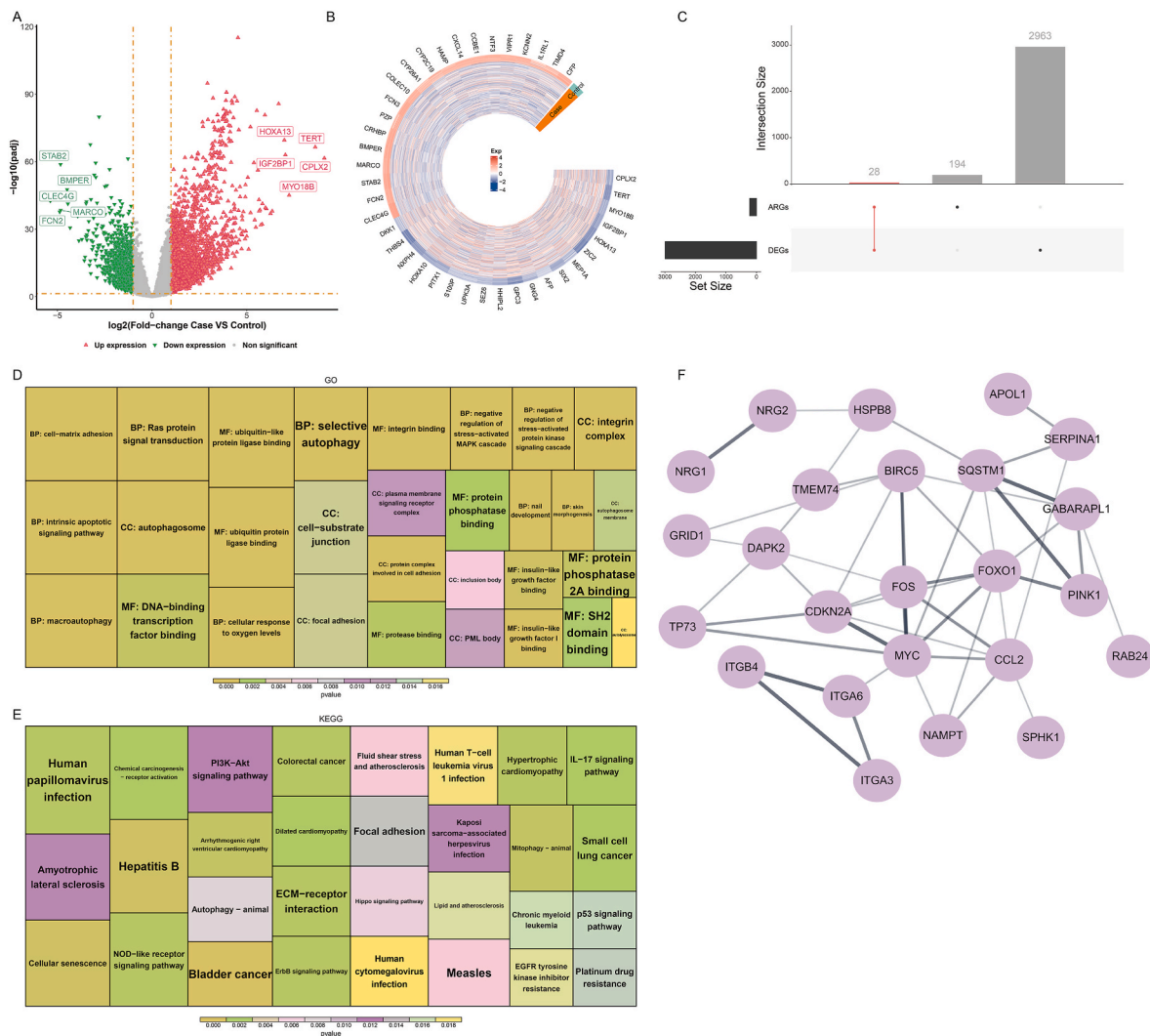


Fig. 2. Analysis and enrichment of DEGs

A) Differential gene expression volcano plot, red represents significant up-regulated genes, green is significant down-regulated genes, grey is non-significant genes. B) The up- and down-regulated TOP20 genes were selected by \log_2FC sequencing, with red representing high expression and blue representing low expression. C) Venn of intersecting genes, with the left bar showing the number of genes in each subset and the top bar showing the number of genes in each intersection. D) GO enrichment results. The size of the box indicates the number of genes enriched, and the colour indicates the significance. E) KEGG enrichment results. Showing TOP30 functional pathways (in order of significance); the size of the box represents the number of genes enriched, and the colour shade indicates significance. F) PPI network analysis.

ab109364, 1:500), anti-HSPB8 (Abcam, ab151552, 1:100), anti-SQSTM1 (Abcam, ab207305, 1:2000).

2.14. qPCR

Total RNA from tissues was extracted using a Trizol reagent (Invitrogen, USA). The extracted RNA was reverse-transcribed (Yeasen, China) and assayed using the kit (ThermoFisher, USA) according to the manufacturer's instructions. The primer sequences are shown in Table 1.

2.15. Statistical analysis

Statistical results were expressed as mean \pm standard deviation, and the number of replications represented is illustrated in the legend. Student's t-test using GraphPad Prism 9 (USA) was used to count the differences between the two groups.

3. Results

3.1. Autophagy-related differentially expressed genes (DE-ARGs) and functional enrichment analysis

The flow of the whole experiment was completed as shown in the figure (Fig. 1). We analysed the differences in gene mRNA expression levels between the HCC and Control groups and screened for differentially expressed genes (DEGs) using $|\log_2FC| \geq 1$ and $P < 0.05$ as criteria (Supplementary Table 2). Our results found that a total of 2991 DEGs were obtained (Supplementary Table 3), including 2026 up-regulated genes (Supplementary Table 4) and 965 down-regulated genes (Supplementary Table 5). Gene differential expression was demonstrated by volcano plots (Fig. 2A), and we selected the top 20 genes to demonstrate expression in HCC and control by heatmaps (Fig. 2B). Subsequently, we intersected with 222 autophagy-related genes (ARGs) and then obtained 28 autophagy-related differential genes (DE-ARGs) (Fig. 2C–Supplementary Table 6). To further understand the biological functions and pathways associated with DE-ARGs, we performed GO and KEGG analyses. In GO, a total of 549 entries were enriched, including 28

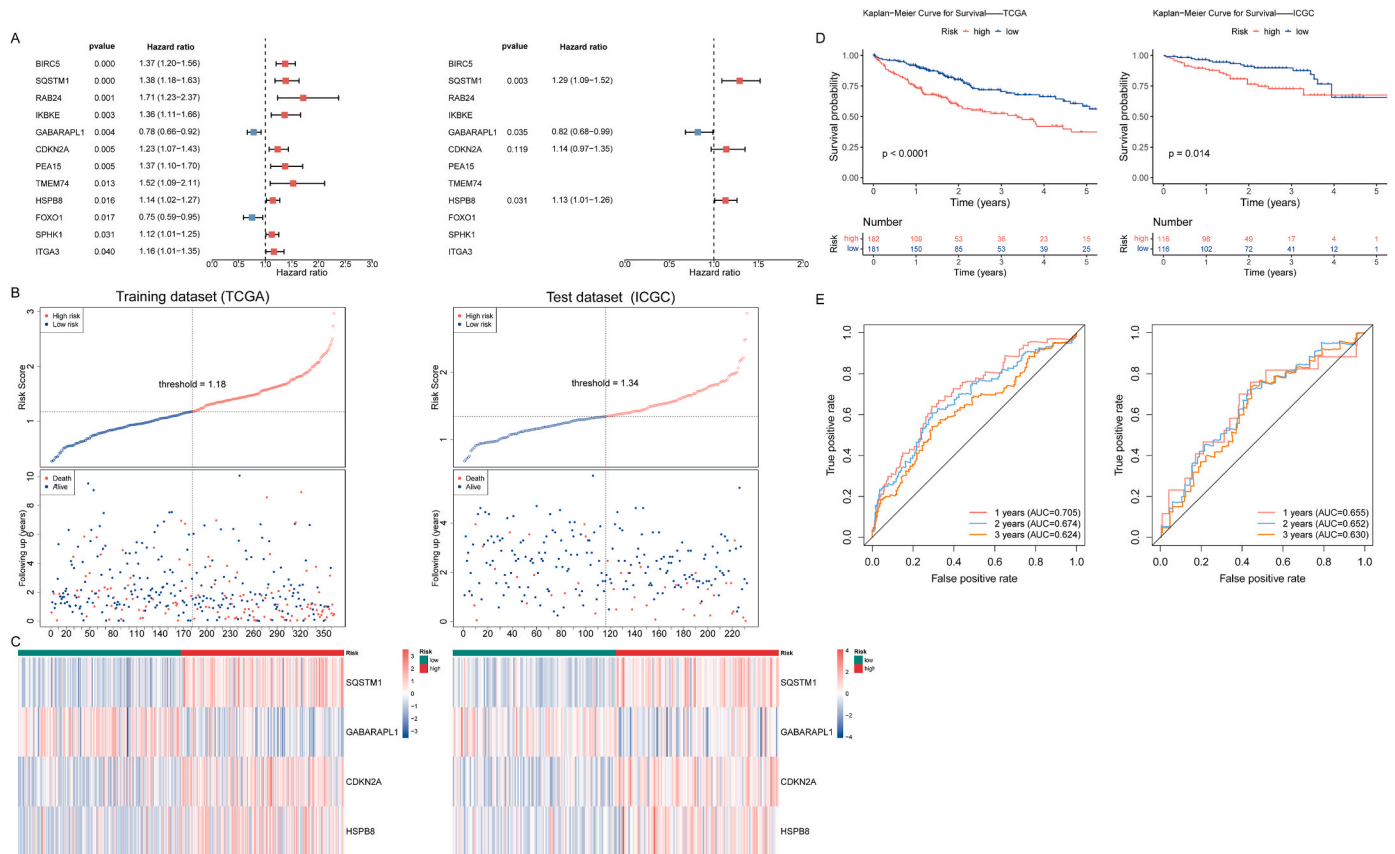


Fig. 3. Risk model construction and assessment

A) Single-factor, multifactor Cox Forest plots. B) Risk curve. The top half of the graph shows the distribution of samples from low to high according to the risk score differentiated by median value. The lower half of the graph shows the corresponding survival status and time of the samples. The vertical coordinate is the survival time. C) Intergroup expression of prognostic genes. D) Survival curves for high and low risk groups. The horizontal coordinate is the survival time, and the vertical coordinate is the survival rate, and the continuous type of step curve plotted to illustrate the relationship between survival time and survival rate. The number in the bottom axis of the graph is the number of samples that survived during the corresponding survival period. E) ROC curve.

CCs, 56 MFs and 465 BPs (Supplementary Table 7). In KEGG, 44 functional pathways were enriched (Supplementary Table 8). Among them, Cellular senescence, Mitophagy-animal, NOD-like receptor signalling pathway and other pathways are related to autophagy (Fig. 2D). Hepatitis B, ECM-receptor interaction, IL-17 signalling pathway, etc., are closely related to the development of hepatocellular carcinoma (Fig. 2E). Finally, we constructed protein-protein interaction (PPI) networks of intersecting genes, which resulted in the identification of 24 genes with interactions (Fig. 2F–Supplementary Table 9), including 47 interacting relationship pairs.

3.2. Screening for prognosis-related genes by cox analysis

We performed univariate Cox regression analyses for the 28 DE-ARGs and screened for genes significantly associated with survival ($p < 0.05$, Supplementary Table 10); we obtained 12 genes (Fig. 3A, Supplementary Table 11). Based on the results of Cox, the Proportional Hazards (PH) Assumption test was performed to screen out the genes ($p > 0.05$). Then, a total of 9 genes (SQSTM1, IKBKE, GABARAPL1, CDKN2A, TME, M74, HSPB8, FOXO1, SPHK1 and ITGA3) passed the selection (Supplementary Table 12). Using multifactorial Cox analysis for further screening. From the risk model construction (Supplementary Table 13), we found a total of 4 model genes (SQSTM1, GABARAPL1, CDKN2A, and HSPB8). Risk scores were calculated with the formula:

$$\text{RiskScore} = \text{SQSTM1} * 0.25 - \text{GABARAPL1} * 0.20 + \text{CDKN2A} * 0.13 + \text{HSPB8} * 0.12.$$

3.3. Assessment of prognostic analyses

Based on the risk scores obtained from the model, the samples were divided into high- and low-risk groups with median values (Supplementary Tables 14 and 15). In both the TCGA training datasets and ICGC validation sets, the number of death samples in the high-risk group was more than in the low-risk group (Fig. 3B). The expression of prognostic genes in groups was shown by heatmap (Fig. 3C). Except for GABARAPL1, which is expressed less in the high-risk group, the expression of the other three genes in the high-risk group is higher than that in the low-risk group. In addition, based on Kaplan-Meier analysis, we found that in both datasets, the survival of high- and low-risk patients' survival was significantly different ($p < 0.05$), with high-risk patients having lower survival than the low-risk group (Fig. 3D). Finally, we assessed the predictive effect of the model by ROC curves. The 1-, 2-, and 3-year survival ROC curves are plotted in the training and validation sets, and we find that the Area Under Curve (AUC) values of 1, 2, and 3 years in the two datasets are higher than 0.6, which indicates that the model has a better prediction effect (Fig. 3E).

3.4. Correlations between prognostic models and clinical factors

To investigate the reliability of the prognostic model in clinical settings, we obtained the following 8 clinical features in the TCGA training set: age, gender, grade, pathologic M, pathologic N, pathologic T, stage

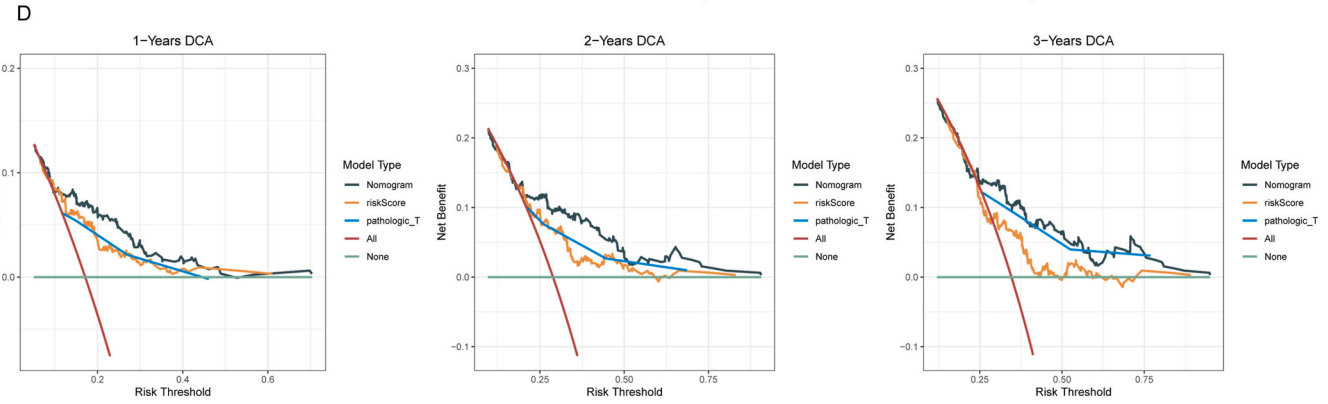
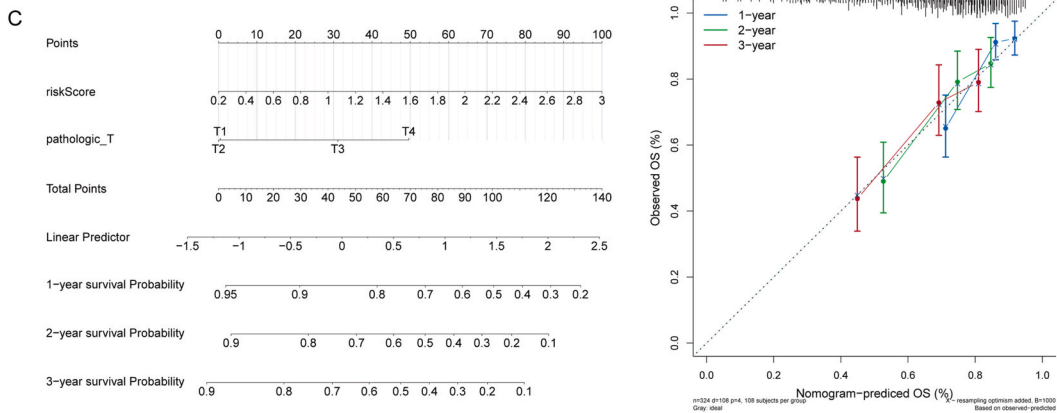
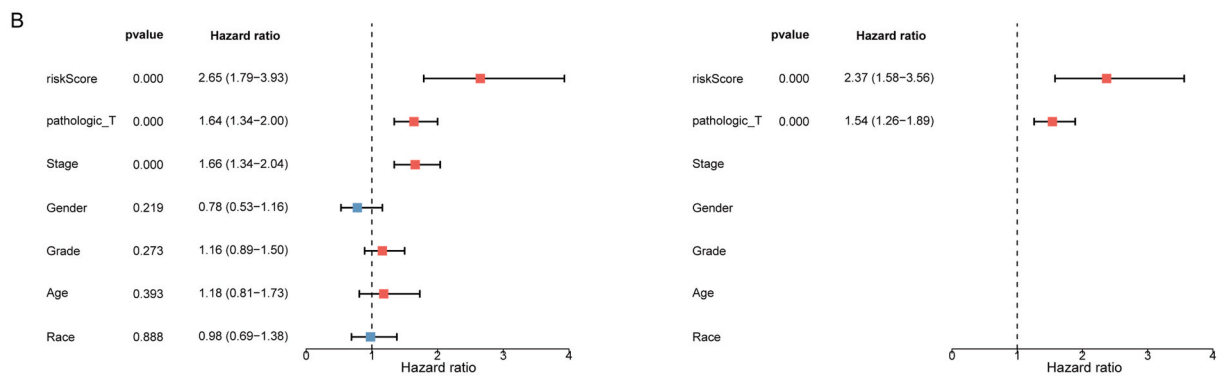
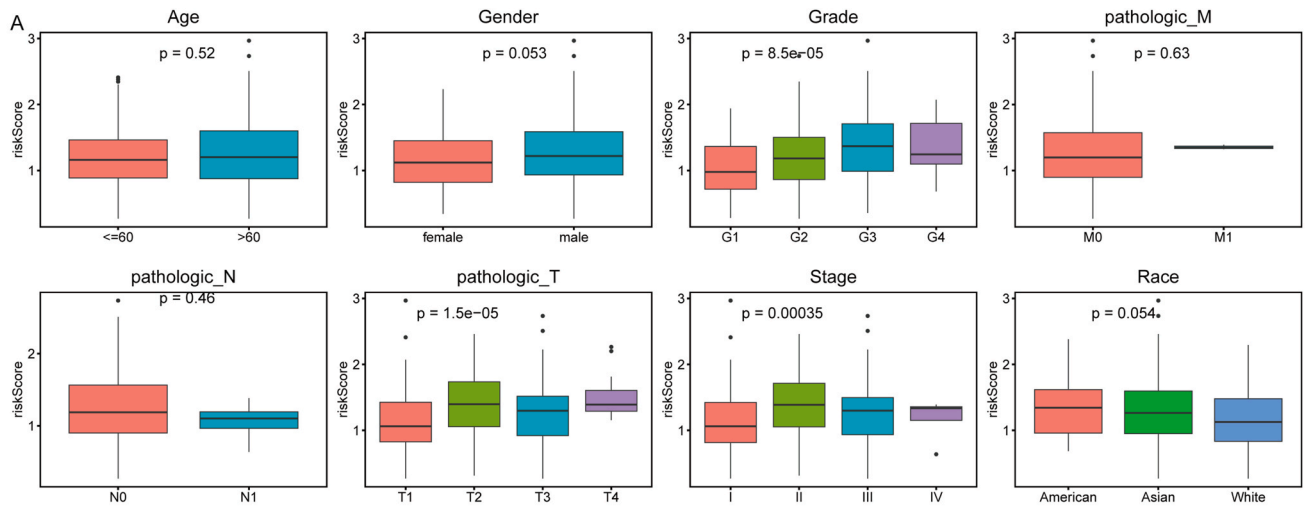


Fig. 4. Clinical trait analysis and alignment diagram
 A) Between-group distribution of risk scores across traits. B) Single-factor Cox Forest plots and multifactor Cox Forest plots. C) Alignment graphs and calibration curves. D) DCA curves for nomogram.

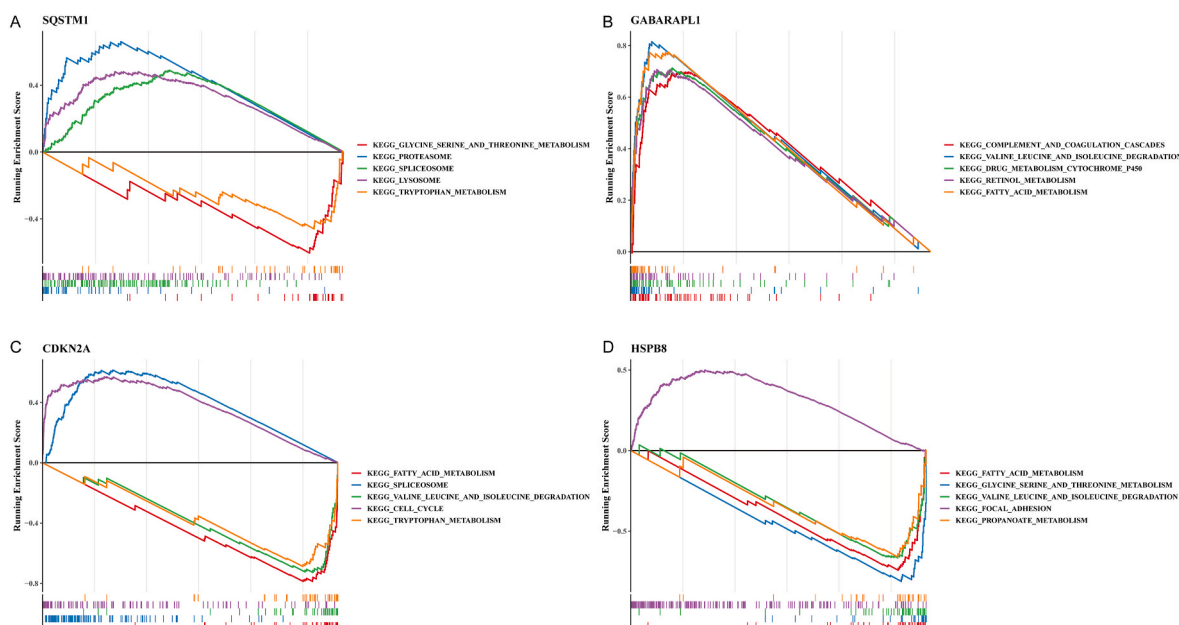


Fig. 5. GSEA enrichment trends of top 5 pathways for model genes

A) The first five enriched pathways of SQSTM1. B) Enrichment pathway analysis of GABARAPL1. C) Pathways enriched in CDKN2A sorted by top 5. D) Enrichment analysis of HSPB8.

and race in the TCGA training set. Through the Wilcoxon rank sum test and the Kruskal-Wallis test, we found that there were significant differences in risk scores between the Grade, pathologic T, and Stage groups ($p < 0.05$) (Fig. 4A, Supplementary Table 16). Subsequently, we used univariate Cox regression and found that risk score, pathologic T, and stage all had a significant effect on patient survival ($p < 0.05$, Supplementary Tables 17 and 18). Based on this result, we performed a multifactorial Cox analysis and obtained 2 significant shapes (risk score, pathologic T) (Fig. 4B–Supplementary Table 19). Finally, we plotted Nomogram plots (Fig. 4C), calibration curves, and Decision Curve Analysis (DCA) curves for 1, 2, and 3 years (Fig. 4D). The calibration curves are close to the diagonal, and the net returns of the column-line plots are all higher than the individual factors, suggesting that the model's predictions are convincing.

3.5. Gene set enrichment analysis (GSEA) of prognosis-related genes

To understand the biological functions and the differences of signalling pathways involved in prognostic-related genes, we performed GSEA analysis with the KEGG gene set as the background. In the TCGA training set, the correlations between prognostic genes and other genes were calculated and ranked separately, and the top 5 enriched pathways were finally selected for presentation. Among them KEGG_TR

YPTOPHAN_METABOLISM, KEGG_CELL_CYCLE and so on were associated with the development of hepatocellular carcinoma (HCC) (Fig. 5A–D, Supplementary Tables 20–23).

3.6. The immune microenvironment of the model

Enrichment scores for 28 immune cells were obtained using the immune-related genes in the Methods section as the background gene set (Supplementary Table 24). In the training set, we used the ESTIMATE algorithm to calculate the scoring traits of the samples. We based on the grouping of the samples in our previous model (high-risk and low-risk groups) to compute how the scores differed between groups. The results obtained a total of 3 scores, StromalScore, ImmuneScore and ESTIMATEScore. The ImmuneScore was significantly different between the two groups ($p < 0.05$) and was lower in the low-risk group than in the high-risk group, while the remaining two scores were not

significantly different between groups (Fig. 6A, Supplementary Table 25). Subsequently, we analysed the differences in the enrichment scores of each immune cell between the groups using the Wilcoxon test. The results showed that the 15 immune cells' enrichment scores significantly differed between the groups ($p < 0.05$, Fig. 6B). Except for Eosinophil, the rest of the significant immune cells were lower in the low-risk group than in the high-risk group. By Spearman correlation analyses of correlations between prognostic genes, risk scores, and immune cell enrichment scores for between-group differences, we found that the risk scores had the highest correlation with Activated CD4 T cells, Natural killer T cells, and Activated Dendritic cells ($r = 0.44, 0.42, 0.33$, Fig. 6C–Supplementary Tables 26–27). Finally, we analysed the differences in the expression of each immune checkpoint between groups based on previous groupings in the TCGA training set. The results showed that there were a total of 51 immune checkpoints that were differently expressed in the two groups (high-risk and low-risk), of which 13, 12, and 14 were receptor, ligand, and antigen-associated immune checkpoints, respectively (Fig. 7). As can be seen from our results, most of the immune checkpoints were expressed less in the low-risk group than in the high-risk group. These results suggest that the grouping of risk models can reflect different immunity levels.

3.7. mRNA expression-based stemness index (mRNAsi) analysis

We quantified the stemness of the tumour samples and calculated the mRNAsi in the training dataset, which reflects the gene expression characteristics of stem cells. The correlation between stemness index and risk score was subsequently analysed, and the results showed that there was a significant positive correlation between stemness index and risk score, with the stemness index in the high-risk group being significantly higher than that in the low-risk group (Fig. 8A, Supplementary Table 28). This means that the risk score can indicate the ability of tumour progression and self-renewal to a certain extent.

3.8. Prediction of drug sensitivity

We used data from the GDSC (Genomics of Drug Sensitivity in Cancer) database to construct a model to predict the IC_{50} values of each drug in the disease samples. Drugs were screened by calculating intergroup

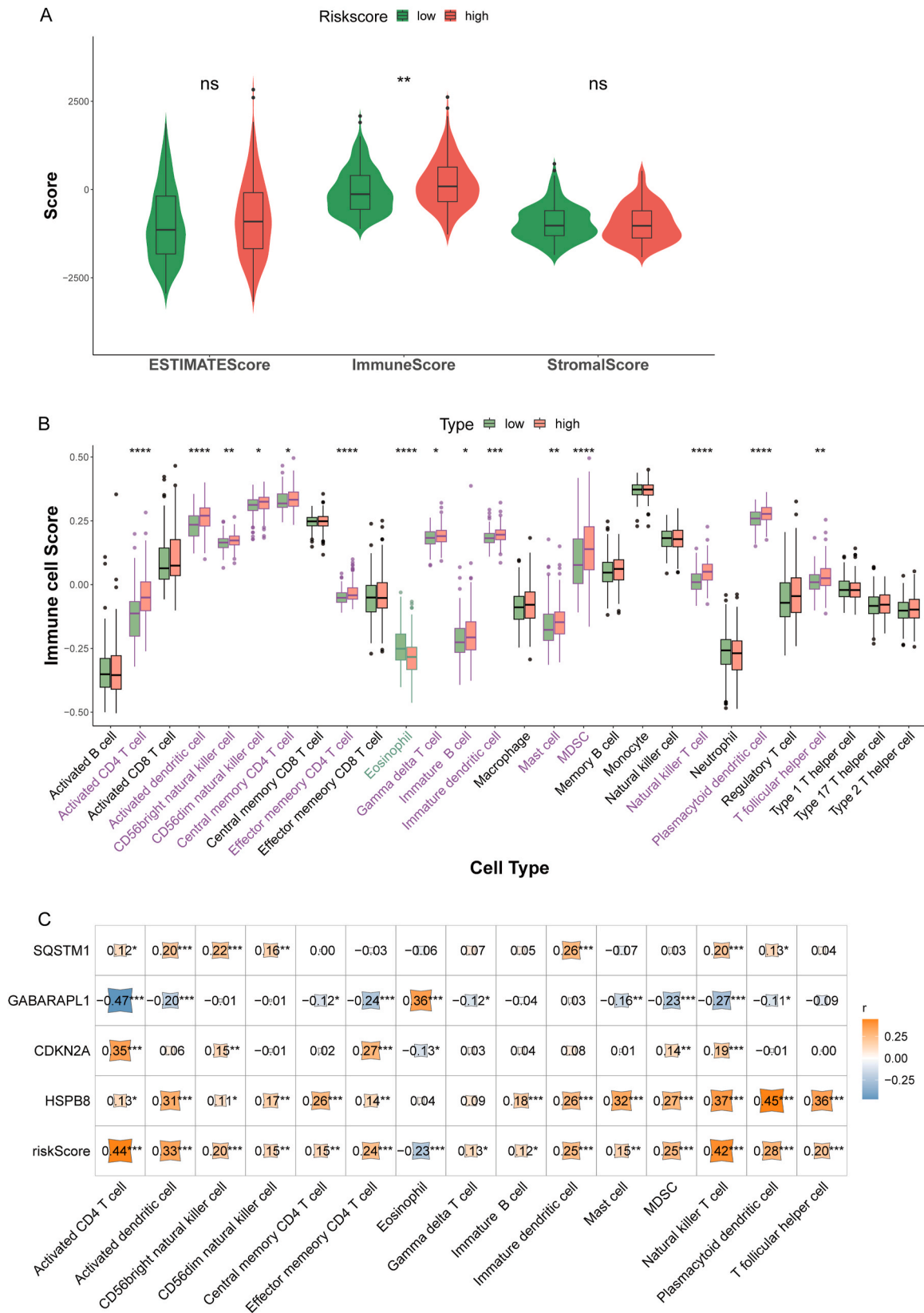


Fig. 6. Immune microenvironmental analysis of key genes

A) Differences between groups in tumour stroma scores. B) Differences in immune cell enrichment scores between groups (purple indicates High > Low, green indicates High < Low, black means not significant). C) Prognostic genes, risk scores and immune cell correlations. ns. $p > 0.05$, * $p \leq 0.05$, ** $p \leq 0.01$, *** $p \leq 0.001$, and **** $p \leq 0.0001$.

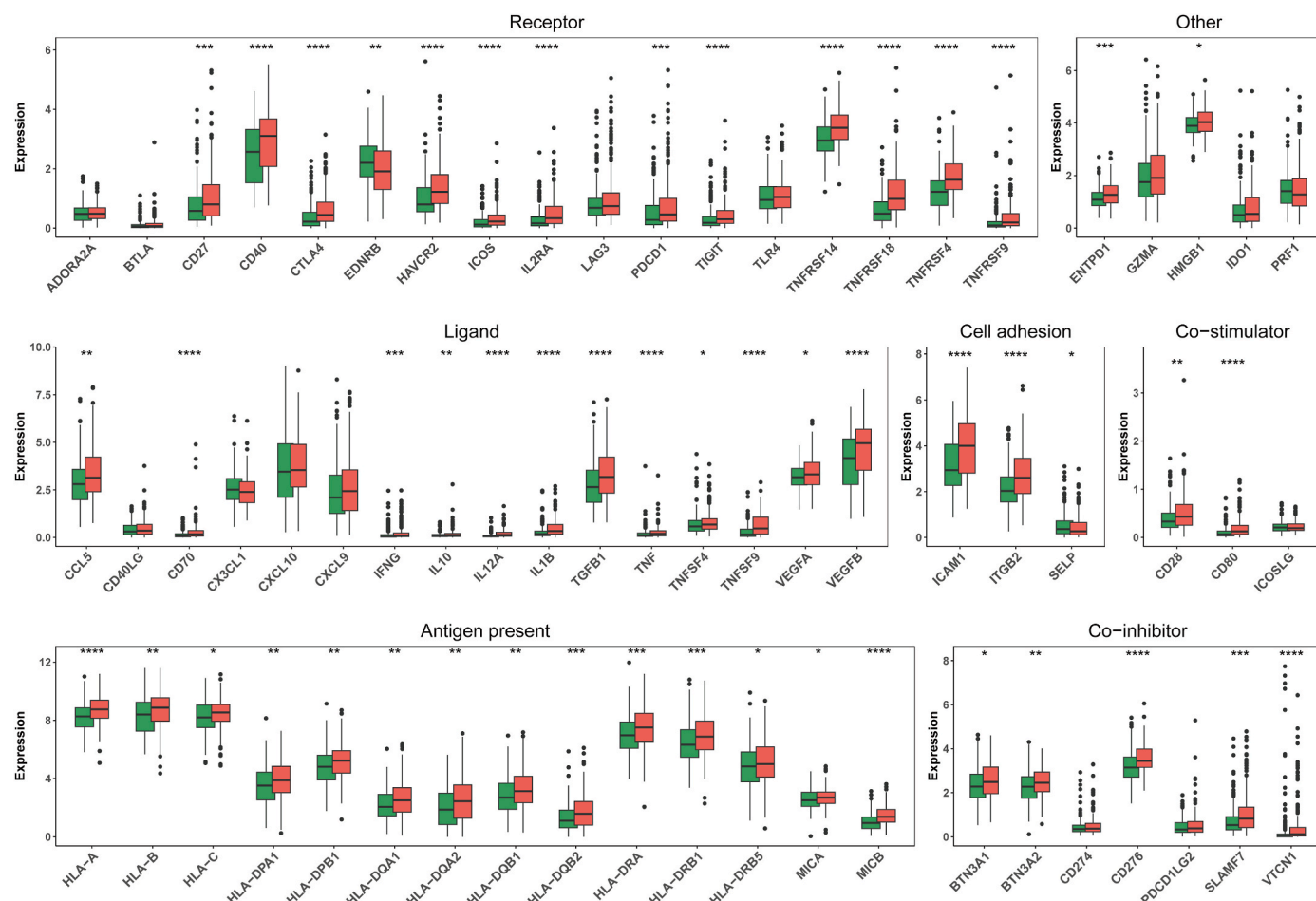


Fig. 7. Differences in immune checkpoint expression between groups. Differences in expression of immune checkpoints between groups. Horizontal coordinates are the immune checkpoints, vertical coordinates are the expression levels, green is the low-risk group, red is the high-risk group, and the top is the difference in the expression levels of the immune checkpoints between the groups. The significance of the difference in the expression level of the immune checkpoints between groups is shown at the top. ns. $p > 0.05$, * $p \leq 0.05$, ** $p \leq 0.01$, *** $p \leq 0.001$, and **** $p \leq 0.0001$.

differences (high- and low-risk groups) in IC_{50} values for all drugs and correlations with risk scores. The screening conditions were 1) significant differences between high- and low-risk groups; 2) absolute correlation between drug IC_{50} values and risk scores ≥ 0.3 . After the analysis, 15 drugs were finally obtained (Fig. 8B–Supplementary Tables 29–31). The results of Sabutoclast show that its IC_{50} value is lower, indicating that a smaller amount of Sabutoclast may have a better inhibitory effect on tumour cells. The IC_{50} value of Sabutoclast in the high-risk group is significantly higher than that in the low-risk group, indicating that low-risk patients have a better response to Sabutoclast treatment.

3.9. Analysis of prognostic gene regulatory networks

We used miRNet, based on the RegNetwork database, to predict four prognostic gene-associated transcription factors (TFs) with degree ≥ 1 , resulting in 61 TFs (Fig. 8C–Supplementary Table 32). We then analysed the regulatory network of competing endogenous RNA (ceRNA) (Fig. 8D). We predicted 4 prognostic gene-related miRNAs and lncRNAs in Starbase. Here, we screened miRNAs with the criterion of being predicted in both miRanda and miRmap databases; then, 56 miRNAs were obtained by filtering (Supplementary Table 33). Predicting miRNA-associated lncRNAs using clipExpNum ≥ 20 as a criterion, we obtained 65 (Supplementary Table 34).

3.10. Validation of prognostic gene expression levels

To further validate the expression of prognostic genes, we analysed the data from the training set. It was found that SQSTM1, CDKN2A, and HSPB8 were up-regulated genes, and GABARAPL1 was down-regulated (Fig. 8E). We used IHC (Fig. 9A–B), western blotting (Fig. 9C–D) and qPCR (Fig. 9E) in 10 HCC samples and their para-cancerous tissues. The experimental results were consistent with our analysis. The full uncropped blots were shown in the supplementary file.

4. Discussion

HCC has always been a hot topic of discussion among cancers. Early diagnosis is effective in reducing the mortality rate of HCC [35]. Most of the clinics use imaging tests, marker tests or puncture tests. Nowadays, treatments for HCC include surgical resection, liver transplantation, chemotherapy and immunotherapy [36]. Most common methods have the best cure rates only for patients with early-stage HCC. Although transcatheter arterial chemoembolisation (TACE) combined with drug therapy improves the overall survival rate for patients in terminal stages [37], the results are still poor compared to early-stage patients. Therefore, the discovery of reliable genes for early diagnosis and treatment of HCC is urgent.

Many studies have shown that inhibition of autophagy brings improvement in clinical outcomes. Models have demonstrated that the combination of anticancer drugs and autophagy inhibitors can have an

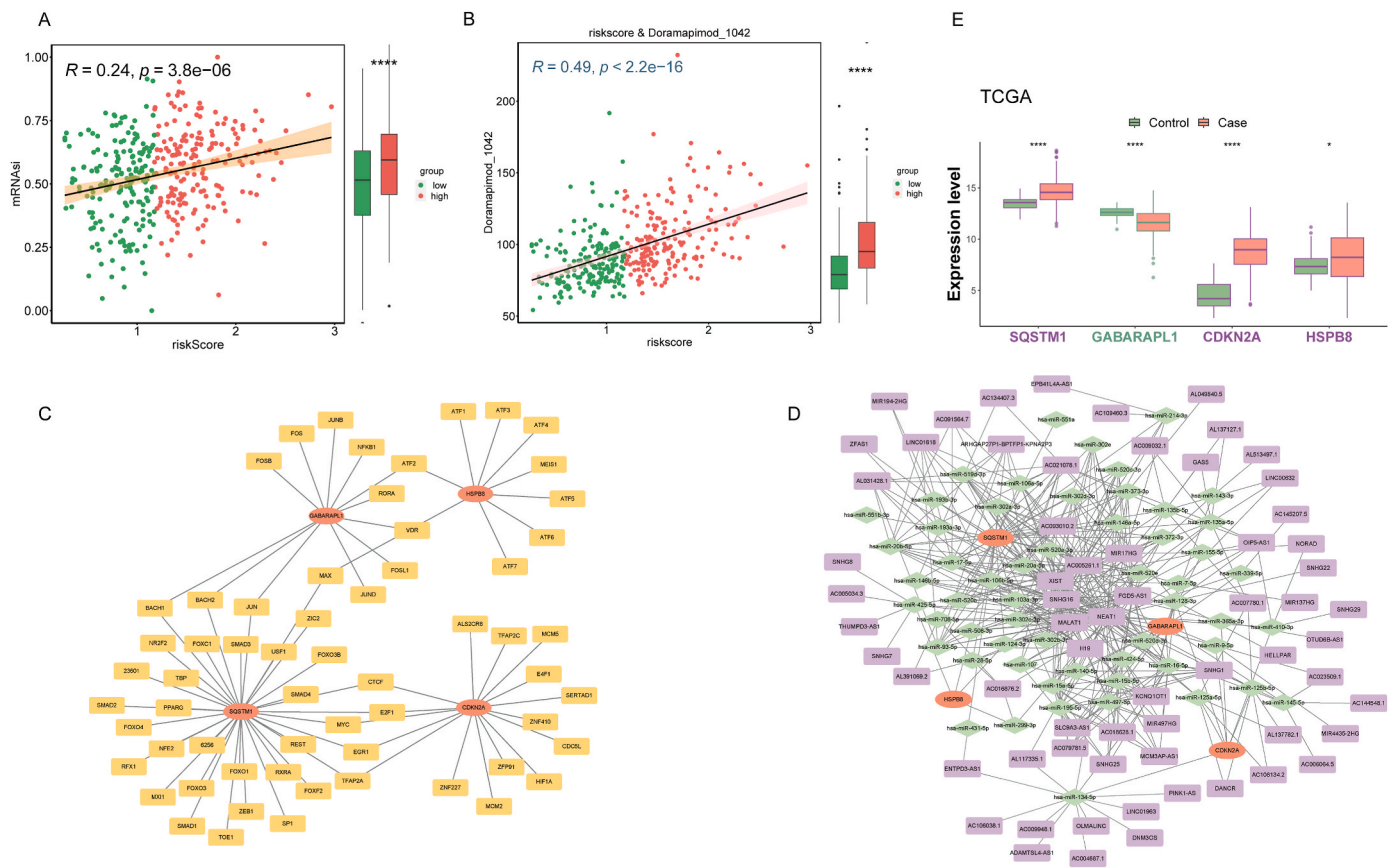


Fig. 8. Further validation of key genes

A) Correlation of mRNAasi with riskScore. B) Correlation between Sabutoclax IC₅₀ values and risk scores and differences between groups. C) TF-mRNA network. The figure shows prognostic genes in red and transcription factors in yellow. D) ceRNA network, prognostic genes in red, miRNAs in green and lncRNAs in purple. E) Intergroup expression of prognostic genes.

anti-tumour effect [38]. A retrospective study illustrates that dysregulation of autophagy is associated with multiple types of cancer progression [39]. It has been illustrated that PARK2 inhibits the development of pancreatic tumours via mitochondrial autophagy [40]. Through the establishment of a mouse model [41], the article demonstrates that autophagy-related gene 7 (Atg 7) deletion leads to abnormalities in autophagy and steatosis in the liver, which ultimately leads to HCC. Herein, we screened DEGs in the normal and HCC groups by differential gene analysis. To further obtain DE-ARGs, we took the intersection of these genes and ARGs to obtain 28 DE-ARGs. GO and KEGG enrichment analyses indicated that DE-ARGs were enriched in signalling pathways closely related to autophagy, such as cellular senescence, Mitophagy-animal, and NOD-like receptor signalling pathway, as well as pathways related to hepatocellular carcinomas, such as hepatitis B, ECM-receptor interactions, and IL-17 signalling. The results of these analyses confirmed the reliability of the candidate genes for further screening of reliable genes in subsequent analyses.

Although the regulatory role of autophagy in cancer is diverse, the mechanisms are becoming clearer with the establishment and validation of different models. Recent studies illustrate that by regulating autophagy-related genes, tumour development can be mediated [42–44]. In our article, after finding HCC and autophagy-related genes, we obtained a total of 9 prognostically relevant genes based on Cox analysis and PH hypothesis testing. Based on further analysis and screening by risk model, we finally obtained 4 genes (SQSTM1, GABARAPL1, CDKN2A, HSPB8). Next, we evaluated the diagnostic value of the four prognostic genes by risk curves, KM curves, and ROC curves. The risk scores were calculated to group and compare the differences in the distribution of survival between the samples. Using risk

curves and heat maps, we found that GABARAPL1 was less expressed in the high-risk group, and the remaining three were more expressed in the high-risk group than in the low-risk group. Subsequently, through validation we found that the AUC values of 1, 2, and 3 years were higher than 0.6, indicating that the model had a better prediction effect. Some previous research reports illustrated the reliability of some prognostic models in HCC and demonstrated the prognostic value of the characterized genes such as AFM, AKR1C3, and GPC3 in HCC by means of multivariate regression models, elastic nets, and columnar plots [45]. Some researchers have also determined the AUC of DEGs by machine learning methods and it has been shown to be useful for early HCC diagnosis [46]. Consistent with our analysis, there are many articles showing the significance of these four key genes in cancer. SQSTM1 is associated with autophagy in lung cancer and is involved in the regulation of lung cancer cell plasticity [47]. In gastric cancer, autophagy regulates important immune checkpoint proteins through SQSTM1, thus regulating the therapeutic effects [48]. Other articles have also demonstrated the regulation of SQSTM1 in HCC, where it binds to a protein, DDX5, thereby stimulating autophagy to ultimately inhibit liver tumour growth [49]. GABARAPL1 regulates hormonal pathways in prostate cancer and is involved in the regulation of autophagy [50]. GABARAPL1 has been shown in other HCC research articles to be associated with poor patient prognosis [51] as well as being a signature gene for mitochondrial autophagy [52]. The regulatory mechanisms of both CDKN2A [53] and HSPB8 [54] in HCC related to autophagy were validated in the stage in the article. In the current study, we used clinical samples to validate the expression of key genes, which was consistent with the database analysis. GABARAPL1 was lowly expressed in tumour samples, whereas CDKN2A, HSPB8 and SQSTM1 were lowly expressed

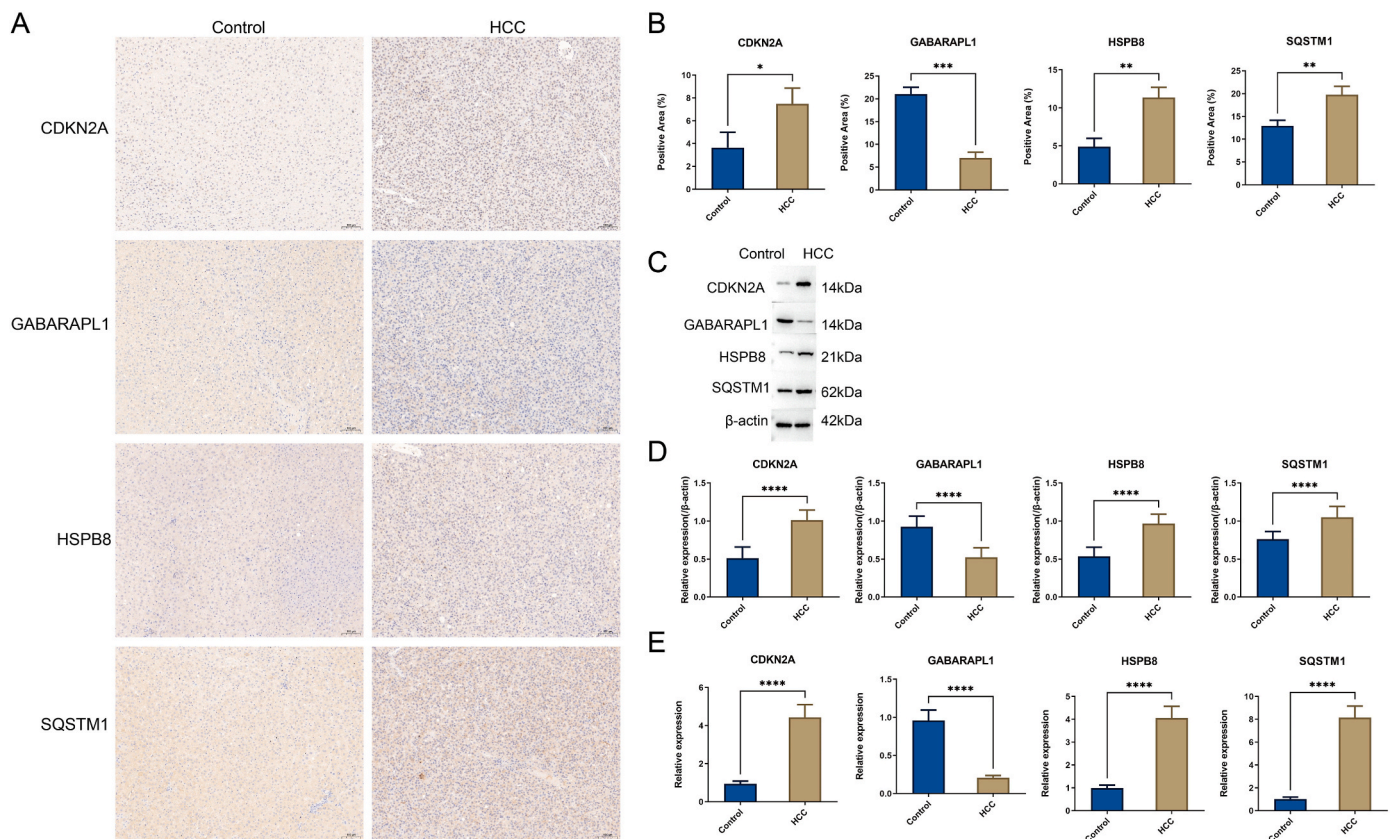


Fig. 9. Validation of expression of key genes in clinical samples

A) Immunohistochemical detection of gene expression, scale bar = 100 μ m, x10, n = 10. B) Statistical results of positive area of IHC. C) Western blotting to detect gene expression, n = 10. D) Statistical results of western blotting. E) qPCR to detect gene expression, n = 10.

in tumours.

Based on the above candidate genes we constructed a risk model. We analysed and found that there was a correlation between the risk score and Grade, pathologic_T, and Stage. Based on the above model, we analysed and found that there was a correlation between the risk score and clinical features such as grading, pathological staging, and inter-staging. Independent prognostic analyses using these clinical traits with correlations were used to construct the nomogram. The nomogram demonstrated better predictive results, which confirmed the potential of the genes we screened for in clinical prognosis. In a previous study, Chen et al. [55] confirmed prognostic genes associated with hypoxia and immunity in pancreatic ductal carcinoma in the same way.

We then analysed the risk score model and the immune environment. We found that the low-risk group had lower immune scores than the high-risk group. By analyzing the immune infiltration of immune cells in each group, we got that among the immune cells with differential expression, the immune cell scores were lower in the low-risk group than in the high-risk group, except for Eosinophil. The study of Wang et al. [56] indicated that the genes related to Eosinophil were biomarkers with prognostic characteristics of HCC. In addition, prognostic genes and risk scores were correlated with immune cells. In our results, risk score and Activated CD4 T cell, Natural killer T cell, Activated Dendritic cell had high correlation. CD4 T cell was also shown to correlate with increased cholesterol in tumour microenvironment in HCC [57]. Natural killer T cell has a complex regulatory role in HCC and is one of the future therapeutic directions [58]. It has been indicated that Dendritic cell activation may be a reliable way to regulate HCC [59]. In addition, we analysed risk scores and immune checkpoints, and the results indicated that the expression of most immune checkpoints was lower in the low-risk group. Immune checkpoints and immune checkpoint inhibitors (ICIs) in HCC are considered to be effective future treatments for HCC

based on immune response [60]. These further confirmed the close association of our risk score with the immune microenvironment. Based on our risk score model, it provides a basis for performing immunotherapy classification.

Cancer stem cells, as a key factor influencing the course of cancer, are thought to contribute to tumour metastasis and influence treatment resistance [61]. Evaluating strategies related to cancer hepatocytes will facilitate the development of additional therapeutic modalities. We next performed stemness index analysis and found that it was significantly and positively correlated with the risk score, suggesting that the risk score can indicate tumour progression and self-renewal ability. Also, we performed a drug correlation analysis based on the risk score and found that low-risk patients had a better response to Sabutoclast treatment. Sabutoclast has been shown experimentally to inhibit cancer stem cells in breast cancer [62]. However, its association with HCC still lacks the support of substantial experimental evidence.

Our study established and evaluated the potential clinical significance of risk modeling in HCC. GABARAPL1, CDKN2A, HSPB8, and SQSTM1 are reliable biomarkers associated with autophagy, and risk models based on them have the potential to diagnose HCC. Despite the reliability of the models indicated by analysis and validation, there are some limitations of the study. For example, there is a lack of cellular or animal models to validate the regulatory mechanisms of key genes. The article is based on database analysis and lacks practical application in clinical settings. Our subsequent study expects further evaluation based on risk modeling. In summary, the autophagy-related prognostic model we constructed may provide new ideas for diagnosing HCC.

Significant statement

Our study identified autophagy-related genes SQSTM1,

GABARAPL1, CDKN2A, and HSPB8 in HCC by bioinformatics analysis. Their prognostic value was evaluated, providing a basis for the discovery of biomarkers and therapeutic targets in liver cancer.

CRedit authorship contribution statement

Yutao He: Writing – original draft, Conceptualization. **Bin Du:** Writing – original draft, Conceptualization. **Weiran Liao:** Writing – original draft, Conceptualization. **Wei Wang:** Data curation. **Jifeng Su:** Formal analysis. **Chen Guo:** Formal analysis. **Kai Zhang:** Resources. **Zhitian Shi:** Writing – review & editing, Conceptualization.

Consent for publication

Not Applicable.

Data availability statement

All data generated or analysed during this study are included in this published article and its supplementary information files.

Ethics statement

The study was approved by the Medical Ethics Committee of the Second Affiliated Hospital of Kunming Medical University.

Funding

This study was supported by the Basic Research Program of Science and Technology Department of Yunnan Province, Project Number: 202201AY070001-109. Research and development of innovative technologies for early screening and precise diagnosis and treatment of liver cancer. Yunnan Provincial Science and Technology Department Key R&D Program (202403AC100023).

Declaration of competing interest

The authors declare that they have no known competing financial interests or personal relationships that could have appeared to influence the work reported in this paper.

Acknowledgements

We appreciate our colleagues for their helpful suggestions.

Appendix A. Supplementary data

Supplementary data to this article can be found online at <https://doi.org/10.1016/j.bbrep.2024.101893>.

Data availability

I have shared the data in supplementary file

References

- [1] K. Oura, A. Morishita, J. Tani, T. Masaki, Tumor immune microenvironment and immunosuppressive therapy in hepatocellular carcinoma: a review, *Int. J. Mol. Sci.* 22 (11) (2021).
- [2] J. Ferlay, M. Colombet, I. Soerjomataram, D.M. Parkin, M. Piñeros, A. Znaor, et al., Cancer statistics for the year 2020: an overview, *Int. J. Cancer* 149 (4) (2021) 778–789.
- [3] Y. Lurie, M. Webb, R. Cytter-Kuint, S. Shteingart, G.Z. Lederkremer, Non-invasive diagnosis of liver fibrosis and cirrhosis, *World J. Gastroenterol.* 21 (41) (2015) 11567–11583.
- [4] M. Chayanupatkul, F. Kanwal, Reply to: "Hepatocellular carcinoma (HCC) in the absence of cirrhosis in patients with chronic hepatitis B virus infection", *J. Hepatol.* 67 (4) (2017) 886–887.
- [5] C. Campbell, T. Wang, A.L. McNaughton, E. Barnes, P.C. Matthews, Risk factors for the development of hepatocellular carcinoma (HCC) in chronic hepatitis B virus (HBV) infection: a systematic review and meta-analysis, *J. Viral Hepat.* 28 (3) (2021) 493–507.
- [6] Y. Sugawara, T. Hibi, Surgical treatment of hepatocellular carcinoma, *Bioscience trends* 15 (3) (2021) 138–141.
- [7] J. Llovet, J. Zucman-Rossi, E. Pikarsky, B. Sangro, M. Schwartz, M. Sherman, et al., Hepatocellular carcinoma, *Nat. Rev. Dis. Prim.* 2 (2016) 16018.
- [8] H. Liu, Y. Yan, R. Chen, M. Zhu, J. Lin, C. He, et al., Integrated Nomogram Based on Five Stage-Related Genes and TNM Stage to Predict 1-year Recurrence in Hepatocellular Carcinoma, vol. 20, 2020, pp. 1–12.
- [9] Z. Yang, Y. Yang, G. Zhou, Y. Luo, W. Yang, Y. Zhou, et al., The prediction of survival in hepatocellular carcinoma based on A four long non-coding RNAs expression signature 11 (14) (2020) 4132.
- [10] M. Russo, G.L. Russo, Autophagy inducers in cancer, *Biochem. Pharmacol.* 153 (2018) 51–61.
- [11] Z. Yue, S. Jin, C. Yang, A.J. Levine, N. Heintz, Beclin 1, an autophagy gene essential for early embryonic development, is a haploinsufficient tumor suppressor, *Proc. Natl. Acad. Sci. U.S.A.* 100 (25) (2003) 15077–15082.
- [12] X.H. Liang, S. Jackson, M. Seaman, K. Brown, B. Kempkes, H. Hibshoosh, et al., Induction of autophagy and inhibition of tumorigenesis by beclin 1, *Nature* 402 (6762) (1999) 672–676.
- [13] Ž. Frangež, Y. Fernández-Marrero, D. Stojkov, S.M. Seyed Jafari, R.E. Hunger, V. Djonov, et al., BIF-1 inhibits both mitochondrial and glycolytic ATP production: its downregulation promotes melanoma growth, *Oncogene* 39 (26) (2020) 4944–4955.
- [14] E. Josset, H. Burckel, G. Noël, P. Bischoff, The mTOR inhibitor RAD001 potentiates autophagic cell death induced by temozolomide in a glioblastoma cell line, *Anticancer Res.* 33 (5) (2013) 1845–1851.
- [15] J.E. Simpson, N. Gammoh, The impact of autophagy during the development and survival of glioblastoma, *Open biology* 10 (9) (2020) 200184.
- [16] L. Li, H. Gao, D. Wang, H. Jiang, H. Wang, J. Yu, et al., Metabolism-relevant molecular classification identifies tumor immune microenvironment characterization and immunotherapeutic effect in cervical cancer, *Front. Mol. Biosci.* 8 (2021) 624951.
- [17] M.I. Love, W. Huber, S. Anders, Moderated estimation of fold change and dispersion for RNA-seq data with DESeq2, *Genome Biol.* 15 (12) (2014) 550.
- [18] K. Ito, D. Murphy, Application of ggplot2 to pharmacometric graphics, *CPT Pharmacometrics Syst. Pharmacol.* 2 (10) (2013) e79.
- [19] Z. Gu, R. Eils, M. Schlesner, Complex heatmaps reveal patterns and correlations in multidimensional genomic data, *Bioinformatics* 32 (18) (2016) 2847–2849.
- [20] J.R. Conway, A. Lex, N. Gehlenborg, UpSetR: an R package for the visualization of intersecting sets and their properties, *Bioinformatics* 33 (18) (2017) 2938–2940.
- [21] G. Yu, L.G. Wang, Y. Han, Q.Y. He, clusterProfiler: an R package for comparing biological themes among gene clusters, *OMICS A J. Integr. Biol.* 16 (5) (2012) 284–287.
- [22] R.A. Zainal-Abidin, N. Afiqah-Aleng, M.R. Abdullah-Zawawi, S. Harun, Z. A. Mohamed-Hussein, Protein-protein interaction (PPI) network of zebrafish oestrogen receptors: a bioinformatics workflow, *Life* 12 (5) (2022).
- [23] A.A. Rizvi, E. Karaesmen, M. Morgan, L. Preus, J. Wang, M. Sovic, et al., gwasurvivr: an R package for genome-wide survival analysis, *Bioinformatics* 35 (11) (2019) 1968–1970.
- [24] T.T. Liu, R. Li, C. Huo, J.P. Li, J. Yao, X.L. Ji, et al., Identification of CDK2-related immune forecast model and ceRNA in lung adenocarcinoma, a pan-cancer analysis, *Front. Cell Dev. Biol.* 9 (2021) 682002.
- [25] P.J. Heagerty, T. Lumley, M.S. Pepe, Time-dependent ROC curves for censored survival data and a diagnostic marker, *Biometrics* 56 (2) (2000) 337–344.
- [26] E. Núñez, E.W. Steyerberg, J. Núñez, [Regression modeling strategies], *Rev. Esp. Cardiol.* 64 (6) (2011) 501–507.
- [27] Z. Zhang, V. Rousson, W.C. Lee, C. Ferdynus, M. Chen, X. Qian, et al., Decision curve analysis: a technical note, *Ann. Transl. Med.* 6 (15) (2018) 308.
- [28] R. Avila, V. Rubinetti, X. Zhou, D. Hu, Z. Qian, M.A. Cano, et al., MyGeneset.info: an interactive and programmatic platform for community-curated and user-created collections of genes, *Nucleic Acids Res.* 51 (W1) (2023) W350, w6.
- [29] L. Zhang, S. Chen, X. Chen, X. Du, H. Liu, Guitar 2: an improved version of the Guitar for sketching the transcriptomic view of RNA-related biological features, *Methods* 203 (2022) 40–45.
- [30] S. Hänzelmann, R. Castelo, J. Guinney, GSVA: gene set variation analysis for microarray and RNA-seq data, *BMC Bioinf.* 14 (2013) 7.
- [31] P. Charoentong, F. Finotello, M. Angelova, C. Mayer, M. Efremova, D. Rieder, et al., Pan-cancer immunogenomic analyses reveal genotype-immunophenotype relationships and predictors of response to checkpoint blockade, *Cell Rep.* 18 (1) (2017) 248–262.
- [32] J. Shi, P. Zhang, H. Su, L. Cai, L. Zhao, H. Zhou, Bioinformatics analysis of neuroblastoma miRNA based on GEO data, *Pharmacogenomics Personalized Med.* 14 (2021) 849–858.
- [33] D. Maeser, R.F. Gruener, R.S. Huang, oncoPredict: an R package for predicting in vivo or cancer patient drug response and biomarkers from cell line screening data, *Briefings Bioinf.* 22 (6) (2021).
- [34] P. Shannon, A. Markiel, O. Ozier, N.S. Baliga, J.T. Wang, D. Ramage, et al., Cytoscape: a software environment for integrated models of biomolecular interaction networks, *Genome Res.* 13 (11) (2003) 2498–2504.
- [35] K. Lv, X. Cao, P. Du, J.Y. Fu, D.Y. Geng, J. Zhang, Radiomics for the detection of microvascular invasion in hepatocellular carcinoma, *World J. Gastroenterol.* 28 (20) (2022) 2176–2183.

- [36] T. Couri, A. Pillai, Goals and targets for personalized therapy for HCC, *Hepatology international* 13 (2) (2019) 125–137.
- [37] J. Arita, A. Ichida, R. Nagata, Y. Mihara, Y. Kawaguchi, T. Ishizawa, et al., Conversion surgery after preoperative therapy for advanced hepatocellular carcinoma in the era of molecular targeted therapy and immune checkpoint inhibitors, *J. Hepato-Biliary-Pancreatic Sci.* 29 (7) (2022) 732–740.
- [38] T. Eckschlager, J. Plch, M. Stiborova, J. Hrabeta, Histone deacetylase inhibitors as anticancer drugs, *Int. J. Mol. Sci.* 18 (7) (2017).
- [39] A.H. Chourasia, K. Tracy, C. Frankenberger, M.L. Boland, M.N. Sharifi, L.E. Drake, et al., Mitophagy defects arising from BNip3 loss promote mammary tumor progression to metastasis, *EMBO Rep.* 16 (9) (2015) 1145–1163.
- [40] C. Li, Y. Zhang, X. Cheng, H. Yuan, S. Zhu, J. Liu, et al., PINK1 and PARK2 suppress pancreatic tumorigenesis through control of mitochondrial iron-mediated immunometabolism, *Dev. Cell* 46 (4) (2018) 441, 55.e8.
- [41] G. Karsli-Uzunbas, J.Y. Guo, S. Price, X. Teng, S.V. Laddha, S. Khor, et al., Autophagy is required for glucose homeostasis and lung tumor maintenance, *Cancer Discov.* 4 (8) (2014) 914–927.
- [42] X. Zhao, Y. Wang, F. Meng, Z. Liu, B. Xu, Risk stratification and validation of eleven autophagy-related lncRNAs for esophageal squamous cell carcinoma, *Front. Genet.* 13 (2022) 894990.
- [43] L. Ruan, W. Chen, X. Zhao, N. Fang, T. Li, Predictive potentials of ZEB1-AS1 in colorectal cancer prognosis and their correlation with immunotherapy, *Journal of oncology* 2022 (2022) 1084555.
- [44] V. El-Khoury, S. Pierson, E. Szwarcbart, N.H. Brons, O. Roland, S. Cherrier-De Wilde, et al., Disruption of autophagy by the histone deacetylase inhibitor MGCD0103 and its therapeutic implication in B-cell chronic lymphocytic leukemia, *Leukemia* 28 (8) (2014) 1636–1646.
- [45] S.F. Zhao, S.G. Wang, Z.Y. Zhao, W.L. Li, AKR1C1-3, notably AKR1C3, are distinct biomarkers for liver cancer diagnosis and prognosis: database mining in malignancies, *Oncol. Lett.* 18 (5) (2019) 4515–4522.
- [46] M. Shi, M.S. Chen, K. Sekar, C.K. Tan, L.L. Ooi, K.M. Hui, A blood-based three-gene signature for the non-invasive detection of early human hepatocellular carcinoma, *Eur. J. Cancer* 50 (5) (2014) 928–936.
- [47] C.C. Miao, W. Hwang, L.Y. Chu, L.H. Yang, C.T. Ha, P.Y. Chen, et al., LC3A-mediated autophagy regulates lung cancer cell plasticity, *Autophagy* 18 (4) (2022) 921–934.
- [48] X. Wang, W.K.K. Wu, J. Gao, Z. Li, B. Dong, X. Lin, et al., Autophagy inhibition enhances PD-L1 expression in gastric cancer, *J. Exp. Clin. Cancer Res. : CR* 38 (1) (2019) 140.
- [49] H. Zhang, Y. Zhang, X. Zhu, C. Chen, C. Zhang, Y. Xia, et al., DEAD box protein 5 inhibits liver tumorigenesis by stimulating autophagy via interaction with p62/SQSTM1, *Hepatology* 69 (3) (2019) 1046–1063.
- [50] C.W. Xie, Y. Zhou, S.L. Liu, Z.Y. Fang, B. Su, W. Zhang, Gabarapl1 mediates androgen-regulated autophagy in prostate cancer, *Tumour biology : the journal of the International Society for Oncodevelopmental Biology and Medicine* 36 (11) (2015) 8727–8733.
- [51] C. Liu, Y. Xia, W. Jiang, Y. Liu, L. Yu, Low expression of GABARAPL1 is associated with a poor outcome for patients with hepatocellular carcinoma, *Oncol. Rep.* 31 (5) (2014) 2043–2048.
- [52] C. Liu, Z. Wu, L. Wang, Q. Yang, J. Huang, J. Huang, A mitophagy-related gene signature for subtype identification and prognosis prediction of hepatocellular carcinoma, *Int. J. Mol. Sci.* 23 (20) (2022).
- [53] T.P.F. Gade, E. Tucker, M.S. Nakazawa, S.J. Hunt, W. Wong, B. Krock, et al., Ischemia induces quiescence and autophagy dependence in hepatocellular carcinoma, *Radiology* 283 (3) (2017) 702–710.
- [54] B. Shu, Y. Zhou, Q. Liang, C. He, F. Li, HSPB8 promoted intrahepatic cholangiocarcinoma progression by enhancing epithelial-mesenchymal transition and autophagy, *Exp. Mol. Pathol.* 123 (2021) 104691.
- [55] D. Chen, H. Huang, L. Zang, W. Gao, H. Zhu, X. Yu, Development and verification of the hypoxia- and immune-associated prognostic signature for pancreatic ductal adenocarcinoma, *Front. Immunol.* 12 (2021) 728062.
- [56] Q. Wang, Z. Zhang, H. Zhou, Y. Qin, J. He, L. Li, et al., Eosinophil-associated genes are potential biomarkers for hepatocellular carcinoma prognosis, *J. Cancer* 15 (17) (2024) 5605–5621.
- [57] M. Wu, X. Zhou, X. Zhou, G. Wang, Y. Zeng, J. Li, et al., ZDHHC3-mediated SCAP S-acylation promotes cholesterol biosynthesis and tumor immune escape in hepatocellular carcinoma, *Cell Rep.* 43 (11) (2024) 114962.
- [58] J. Ning, Y. Wang, Z. Tao, The complex role of immune cells in antigen presentation and regulation of T-cell responses in hepatocellular carcinoma: progress, challenges, and future directions, *Front. Immunol.* 15 (2024) 1483834.
- [59] J. Cao, B. Su, C. Zhang, R. Peng, D. Tu, Q. Deng, et al., Degradation of PARP1 by MARCHF3 in tumor cells triggers cCAS-STING activation in dendritic cells to regulate antitumor immunity in hepatocellular carcinoma, *Journal for immunotherapy of cancer* 12 (11) (2024).
- [60] B. Sangro, P. Sarobe, S. Hervás-Stubbs, I. Melero, Advances in immunotherapy for hepatocellular carcinoma, *Nat. Rev. Gastroenterol. Hepatol.* 18 (8) (2021) 525–543.
- [61] L.H. Huang, S.C. Wu, Y.W. Liu, H.T. Liu, P.C. Chien, H.P. Lin, et al., Identification of crucial cancer stem cell genes linked to immune cell infiltration and survival in hepatocellular carcinoma, *Int. J. Mol. Sci.* 25 (22) (2024).
- [62] Y. Hu, E. Yagiie, J. Zhao, L. Wang, J. Bai, Q. Yang, et al., Sabutoclax, pan-active BCL-2 protein family antagonist, overcomes drug resistance and eliminates cancer stem cells in breast cancer, *Cancer Lett.* 423 (2018) 47–59.